Pressure induced magnetic phase separation in $La_{0.75}Ca_{0.25}MnO_3$ manganite.

M. Baldini,[1,2] L. Capogna,[3] M. Capone,[4,1] E. Arcangeletti,[1] C. Petrillo,[5,4] I. Goncharenko,[6] and P. Postorino[1,4]

[1] *Dipartimento di Fisica, Università "Sapienza", P.le A. Moro 4, 00187 Roma, Italy*
[2] *HPSynC, Geophysical Laboratory, Carnegie Institution of Washington, 9700 S. Cass Avenue, Argonne, IL 60439, USA*
[3] *Consiglio Nazionale delle ricerche IOM-OGG c/o Institut Laue Langevin 6 rue J. Horowitz 38042 Grenoble, France*
[4] *Consiglio Nazionale delle Ricerche, Istituto Officina dei Materiali (CNR/IOM), Uos Democritos, SISSA, International School for Advanced Studies (SISSA/ISAS), Via Bonomea 265, 34136 Trieste, Italy*
[5] *Dipartimento di Fisica, Università di Perugia, 06123 Perugia, Italy*
[6] *Laboratoire Léon Brillouin, CEA-CNRS, CE-Saclay, 9191 Gif-sur-Yvette, France*

The pressure dependence of the Curie temperature $T_C(P)$ in $La_{0.75}Ca_{0.25}MnO_3$ was determined by neutron diffraction up to 8 GPa, and compared with the metallization temperature $T_{IM}(P)$ [8]. The behavior of the two temperatures appears similar over the whole pressure range suggesting a key role of magnetic double exchange also in the pressure regime where the superexchange interaction is dominant. Coexistence of antiferromagnetic and ferromagnetic peaks at high pressure and low temperature indicates a phase separated regime which is well reproduced with a dynamical mean-field calculation for a simplified model. A new P-T phase diagram has been proposed on the basis of the whole set of experimental data.

PACS numbers: 75.47.Lx, 62.50.-p, 64.75.Qr

Perovskite-like manganites $La_{1-x}Ca_xMnO_3$ (LaCax) exhibit a variety of physical properties depending on the Ca concentration x. The strong correlation among magnetic, electronic, orbital and transport properties of manganites makes these systems particulary sensitive to external perturbations, such as temperature variation, application of magnetic field or high pressure (HP) [1, 2]. The most popular phenomenon is the Colossal Magneto-Resistance (CMR) [3] observed over the $0.2 < x < 0.5$ range. Here, the system shows a transition from a high temperature paramagnetic (PM) insulating phase to a low temperature ferromagnetic (FM) metallic one and its properties can be described by two competing mechanisms: double-exchange (DE) [4] mechanism and Jahn-Teller (JT) effect [5]. The DE model, which couples magnetic and electronic degrees of freedom, qualitatively explains the observed transition and the contiguity between the insulator to metal transition temperature T_{IM} and the Curie temperature T_C. More realistic modeling is only obtained by introducing the JT mechanism with its charge localizing effect [5].

HP techniques were successfully employed to investigate the role of JT structural distortion on manganite properties. The idea is that lattice compression reduces JT distortion [6, 7], increases hopping integral t, thus favoring the onset of metallic phase [8]. Several manganites show indeed an increase of T_{IM} on applying pressure up to 2-3 GPa [9, 10]. Nevertheless, experiments at higher pressures cast doubts on the above scheme [11, 12]. Several HP experiments were carried out on LaCax manganites. In particular, in LaCa0.25 T_{IM}(P) was found to increase linearly only up to P$\simeq$ 3 GPa, to bend down above 6 GPa and to approach an asymptotic value close to room temperature [8, 13]. An antiferromagnetic (AFM) superexchange (SE) interaction between the Mn magnetic moments [14], which are formed by localized t_{2g} electrons, was proposed to be responsible for the anomalous $T_{IM}(P)$ evolution at HP [15]. This peculiar pressure behavior can be ascribed to a competition between the DE and the SE interaction, which, is responsible for AFM order observed away from the CMR concentration region at ambient pressure. Since the strength of DE is proportional to the hopping integral t and SE is proportional to t^2, on increasing pressure (i.e. t) the role of SE versus DE is continuously enhanced and it is expected to become the dominant interaction in the HP regime [8, 15]. The pressure dependence of the magnetic transition was recently investigated by neutron diffraction in LaCa0.33 [16] and LaCa0.25 [17] over the $0-4$ GPa range and an almost linear P-dependence of T_C was observed. In LaCa0.25 rather close values of T_{IM} and T_C [17] were found over the whole P range. As a confirm of the role of SE, evidence of AFM order coexisting within the FM phase was also obtained at low temperature and HP [16, 17]. The suppression of the long range FM order at HP (around 23 GPa) in LaCa0.25 was deduced by X-ray magnetic dichroism data [18]. The remarkable compression of MnO_6 octahedra along the b axis and the anomalous change in the lattice strain at around 23 GPa together with the monotonic decrease of the FM moment with pressure, suggested indeed a transformation from an orbitally disordered FM phase to an orbitally ordered AFM phase [18]. The coexistence of the two magnetic phases in the pressure range between 2 and 23 GPa was conjectured [18]. It is worth to note that although the tendency toward mixed phases, whether structural or magnetic, was recently observed in several manganites at ambient [19] and high pressure [6, 20–22], the theoretical investigation of this phenomenon was rather limited.

Although LaCa0.25 is the most extensively investigated manganite system under pressure, no experimental data are available on $T_C(P)$ over the P range where

T_{IM} is no more linear and the SE mechanism is dominant over the DE. In the present paper we extend the neutron diffraction measurements on LaCa0.25 up to 8 GPa in order to clarify the role and the relative strength of DE and SE interactions and the coupling between T_C and T_{IM} in HP regime. The tendency towards phase separation is modeled by using the simple theoretical approach successfully employed in Ref. [15].

The neutron diffraction experiment was carried out at the LLB (Saclay, FR) using the G6 − 1 two-axis powder diffractometer with a selected incident neutron wavelength λ = 4.74 Å. The diffraction patterns were collected over the 1.5-300 K temperature range along several isobaric paths. Details about the cell are reported in Ref. [23]. Sapphire anvil were used at 2.1, 3.9, and 6.0 GPa and, diamond anvils were employed at 8 GPa. The sample volume ranged from several millimeters (sapphire anvils) to 0.01 mm^3 (diamond anvils). The sample, prepared by a solid reaction method, was finely milled and a mixture of sample and NaCl salt (1:2 volume proportion) was loaded in the gasket hole together with small ruby spheres for pressure calibration.

Ambient pressure data were collected over a wide d-space range 2.5 Å $< d <$ 54 Å ($2\theta = 5 - 140°$) using two detector positions. Diffraction patterns at high and low temperature are shown in the inset of Fig.1(a). At low temperature, the strong increase of the peak intensities at d=3.87 $\mathring{A}$ ((1 0 1)/(0 2 0)) and d=2.74 $\mathring{A}$ ((2 0 0)(0 0 2)(1 2 1)) can be ascribed to the FM contribution [17] (inset of Fig.1(a)). The diffraction pattern was thus refined using the Pnma orthorhombic structure with an associated FM order. The lattice parameters (a=5.47 $\mathring{A}$, b=7.72 $\mathring{A}$, c=5.50 $\mathring{A}$) and the magnetic moment $\mu = 3.57\mu_B$ obtained at ambient pressure by Rietveld refinement are in good agreement with the results of Ref. [24].

In order to reduce the acquisition time at HP, we focused on the main peak at d=3.87$\mathring{A}$ and diffraction patterns were collected exploiting only one detector position ($2\theta = 12 - 91°$ and 3.3 $\mathring{A} < d <$ 22 $\mathring{A}$). Data collected at 6 GPa are shown in Fig.1(b) where new magnetic reflections are found at d=7.38 $\mathring{A}$ (0 1 0) and d=3.47 $\mathring{A}$ (1 1 1). These peaks are unambiguously observed at P= 3.9 GPa and upwards, whereas the data collected at P= 2.1 does not allow any definitive conclusion. Nevertheless, a new pressure induced peak (d=7.47 $\mathring{A}$ at 1.5 GPa) was previously reported in Ref.[17] and ascribed to an AFM order with A-type structure and propagation vector k = (000). This suggests that the AFM peak is probably too weak compared with the signal/noise ratio to be observed in the patten collected at P= 2.1 GPa.

Looking at the present data, a discrepancy is observed between the observed AFM peak position and the expected d-spacing calculated on the basis of the lattice parameters. For example, considering the lattice parameters ((a=5.41$\mathring{A}$, b=7.66$\mathring{A}$ c= 5.45$\mathring{A}$).) obtained at 6 GPa, the (0 1 0) AFM peak is expected to be found at 7.66 $\mathring{A}$, whereas it is centered at d=7.38 $\mathring{A}$ (see Fig.1 (b)). At this point, it is worth noticing that both Kozenklo and

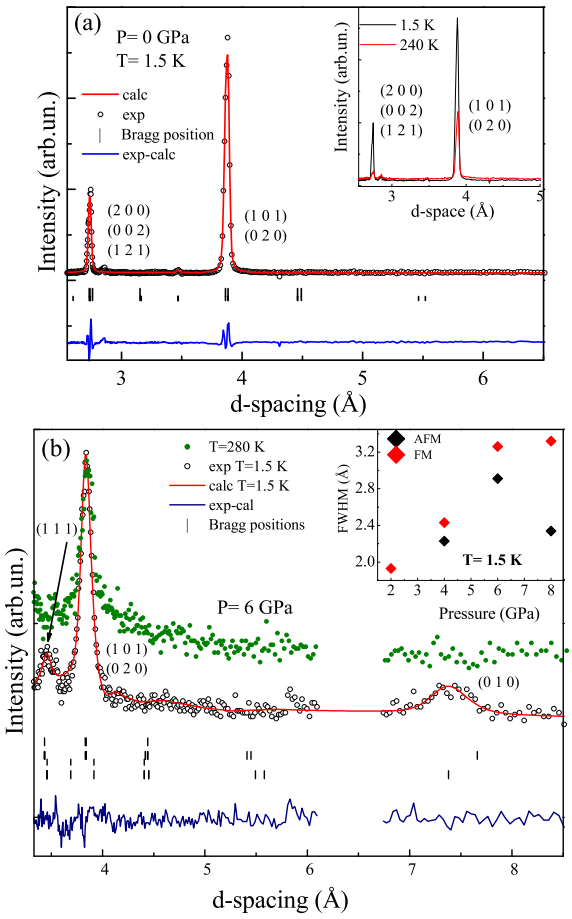

FIG. 1: (a): Diffraction pattern and Rietveld refinement at P=0 and T=1.5 K. Inset: comparison between the P=0 diffraction patterns collected at T=240 and 1.5 K. (b) Diffraction patterns at 6 GPa collected at T=280 and 1.5 K. Peaks at d = 3.47 and d = 7.38 Å are ascribed to AFM order. Calculated positions of the Bragg reflections are also shown: the two upper sets correspond to the nuclear and magnetic phase in agreement with Ref.[17, 18], the two lower sets are associated to the second structural and magnetic phase. Inset: FWHM of AFM and nuclear peaks versus pressure at T=1.5 K.

Ding observed an uniaxial anisotropic compression of the MnO_6 octahedra along the b axis of the orthorhombic structure, which is consistent with this shift of the AFM peak position [17, 18]. These findings suggest that the two magnetic phases, the AFM and the FM, are not associated to the same nuclear phase. Two possible explanations can be proposed: i) the AFM order is not commensurate with the nuclear phase, as already reported for some manganite compounds [25]; ii) the AFM order is associated to a nuclear phase with the same Pnma symmetry but different values of lattice parameters.

In support of the ii) hypothesis, the positions of nuclear and magnetic reflections were obtained above 4 GPa using Fullprof software (see Fig.1(b)) [26]. For example at 6 GPa, two Pnma nuclear structures and two magnetic

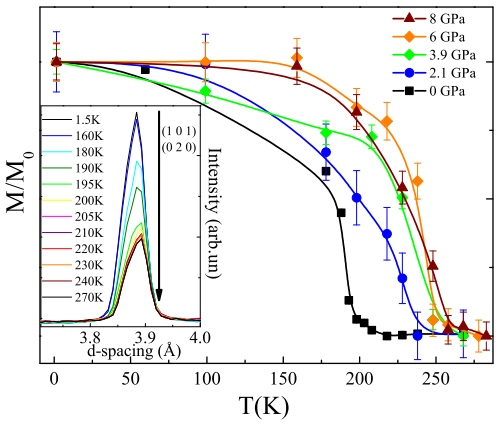

FIG. 2: Normalized magnetic moments versus temperature (solid lines are guides to the eye). Inset: temperature dependence of the FM peak h,k,l=1,0,1

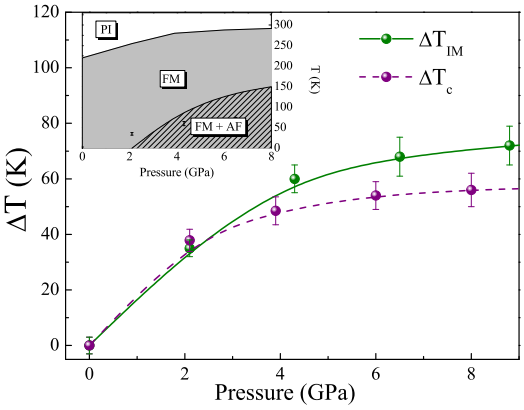

FIG. 3: Temperature variation of T_C and T_{IM} [8] versus pressure. Inset: tentative P-T phase diagram. The onset of the AFM peak at 2 GPa refers to Kozenklo *et al.* work [17]

orders were considered: the first one associated to FM order with the set of lattice parameters reported in Ref. [17, 18]) and the second one associated to an AFM order with a=5.58 $\AA$, b=7.38 $\AA$ and c=5.49 $\AA$. The AFM unit cell was described by four Mn atoms: $Mn_1 = (00\frac{1}{2})$, $Mn_2 = (\frac{1}{2}00)$ $Mn_3 = (0\frac{1}{2}\frac{1}{2})$ $Mn_4 = (\frac{1}{2}\frac{1}{2}0)$. The magnetic structure is a combination of the Γ_5 and Γ_7 representations. Bragg reflections calculated for the AFM structure (A-type) using the $R_x = (++--)$ and $R_y = (++--)$ sequence of magnetic moments and propagation vector $k = (000)$, were well consistent with the experiment as shown in Fig.1(b). The magnetic moments lay on the ab plane and they are placed in a way that is similar to that one observed in $LaMnO_3$ at high pressure [27]. The fractional volumes of the FM and the AFM phases were obtained for the neutron pattern collected at T= 5K and were found to pass from 87.9 % (FM) and 12.1 % (AFM) at 4 GPa to 76.3 % (FM) and 23 % (AFM) at 8 GPa. The FWHM of the FM (101)/(020), and the AFM peak (010), show opposite behaviors on increasing the pressure: the former increases while the latter decreases (see the inset of Fig.1(b)). This behavior is thus consistent with the hypothesis ii), that is lattice compression simultaneously induces both AFM order and a separation between two isostructural nuclear phases.

The emerging scenario is consistent with a founded physical picture. If AFM order is driven by SE interaction, Mn orbitals are expected to order in a way that reduces b axis. The connection between lattice and orbital degrees of freedom, as investigated in several orthorhombic manganites [21, 28, 29], suggests that the development of orbital ordering results in a contraction of b parameter, and if $b/\sqrt{2} < c < a$ the occurrence of an orbital ordering can be conjectured [28, 29]. On the other hand, if $c > a \simeq b/\sqrt{2}$, orbital disorder is expected. It appears thus reasonable to associate FM and AFM order to orthorhombic phases with large and small b parameters: 7.66 $\AA$ and 7.38 $\AA$ respectively.

The FM to PM transition can be identified looking at the temperature dependence of the integrated intensity of the main peak (d=3.87$\AA$) (inset in Fig. 2). The results of the refinements do not considerably change including or excluding the Debye-Waller factor suggesting that the temperature dependence of the nuclear intensities can be neglected. Therefore, the Debye-Waller factor was neglected over the scattering vector range relevant to magnetic peaks. After proper background correction, the integrated peak intensities, subtracted by the nuclear contribution, can be reasonably considered proportional to the effective magnetic moments M. The temperature dependence of the normalized magnetic moments M/M_0 (where M_0 is the effective magnetic moment at the lowest T) is shown in Fig.2 at different pressures.

A rapid increase of T_C on applying pressure is evident over the low pressure range (0-4 GPa), whereas a strongly reduced pressure dependence is observed above 4 GPa. We notice that the observed broadening of the transition can be likely ascribed to strain effects due to pressure gradients. The data were analyzed using a modified Brillouin function to describe the temperature dependence of the magnetization, according to the Weiss molecular field theory [30]. To avoid the intrinsic ambiguity of the definition of both T_C and T_{IM}, we used the temperature variations ΔT from ambient pressure $T_C(P=0)$ and $T_{IM}(P=0)$ to compare the pressure dependence of $T_C(P)$ and $T_{IM}(P)$ [8]. As shown in Fig. 3, the pressure dependence of ΔT is basically the same for both T_C and T_{IM}: a linear increase at low pressure followed by a saturation towards an asymptotic value, above 6 GPa. This result further confirms the onset of a pressure driven localizing mechanism that, becoming competitive with DE delocalizing mechanism at high pressure, strongly affects both the transition temperatures T_C and T_{IM}. Moreover, the onset of an AFM state at low temperature coexisting with the FM order confirms the SE-AFM nature

of the localizing interaction. This suggests a phase separation scenario at low temperature, as depicted in the inset of Fig. 3 where a tentative P-T phase diagram is shown. We finally notice that $\Delta T_C(P)$ slightly deviates from $\Delta T_{IM}(P)$ only at very high pressure. This means that decreasing temperature at a pressure above ~ 4 GPa, LaCa0.25 enters a metallic phase before achieving the FM state. This features might be consistent with a percolation scenario among metallic clusters in a PM insulating bulk, as previously suggested by HP optical measurements [20].

In order to understand theoretically if the pressure-induced increase of AFM-SE can, in turn, induce a phase separation, we considered a simplified model for manganites similar to that used in Refs. [15, 31].

$$\begin{aligned} H &= -t \sum_{\langle ij\rangle\sigma} \left(c^\dagger_{i,\sigma} c_{j,\sigma} c^\dagger_{j,\sigma} c_{i,\sigma} \right) - \mu \sum_{i\sigma} c^\dagger_{i\sigma} c_{i\sigma} + \\ &- J_H \sum_i \vec{\sigma}_i \cdot \vec{S}_i + \\ &+ J_1 \sum_{\langle ij\rangle} \vec{S}_i \cdot \vec{S}_j - g \sum_i (n_i)\,(a_i + a^\dagger_i) + \omega_0 a^\dagger a. \end{aligned} \quad (1)$$

A single band of itinerant electrons with nearest-neighbor hopping t replaces the two e_g bands, and a Holstein coupling to a local Einstein phonon of frequency ω_0 mimics the JT interaction. The DE physics is introduced through an FM coupling between the itinerant band and localized spins $\vec{S}_i$ associated to the t_{2g} orbitals. The localized spin are, in turn, antiferromagnetically coupled with a coupling constant which is small at ambient pressure and grows with increasing pressure ad discussed in Ref. [15]. We work in the grandcanonical ensemble, where the chemical potential μ determines the particle density in the e_g bands. The density $n = \langle \sum_{i\sigma} n_{i,\sigma} \rangle$, where $n_{i,\sigma} = c^\dagger_{i,\sigma} c_{i,\sigma}$ is related to the Ca doping by the relation $x = 1 - n$

The study of the thermodynamic instability associated to phase separation requires to work in the thermodynamic limit, which can be addressed using dynamical mean-field theory (DMFT)[32]. We studied the Holstein-DE model (1) at T=0 using DMFT and exact diagonalization to solve the numerical part of DMFT. We used our implementation of DMFT, as discussed in Ref. [33], with exact diagonalization using 8 levels in the discretized bath.

Since the aim of this calculation is to understand if, on general grounds, phase separation can be expected from the competition between AFM and FM, we introduced some safe approximations. In particular we treated the localize t_{2g} spins as classical variables neglecting quantum fluctuations. Moreover, in light of the experimental suggestions, only the two configurations FM and commensurate AFM ordering were considered, neglecting intermediate orientations and more exotic spin patterns. We computed the total energy for these two phases and

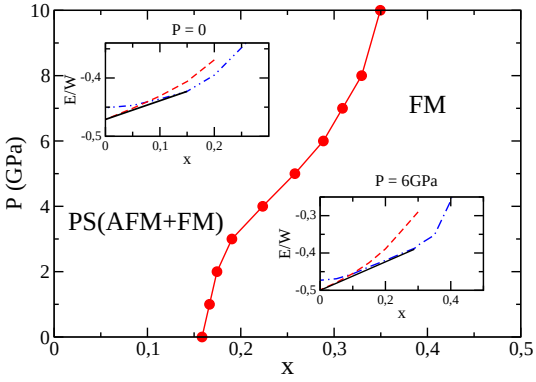

FIG. 4: P-x phase diagram for the Holstein-DE model with parameters from Ref.[15]. A pressure dependence line separates a phase separation region from a homogeneous ferromagnetic state. Phase separation is favored by increasing pressure. Insets: the x-dependence of the Free Energy normalized to the bandwidth at P=0 and 6 GPa. Dashed red (blue) line represents the x-dependence for the AFM (FM) phase. Solid black line is a Maxwell construction whose boundaries determine the doping range for which phase separation takes place at the chosen pressure.

for the nonmagnetic phase as a function of the Ca concentration. The effect of pressure has been included in the calculations adopting the parameters of Ref. [15], with the SE coupling scaling as the square of the hopping parameter. Even though our model is too simplified to attempt a quantitative comparison with the experimental phase diagram, it is expected to properly reproduce the competition between magnetic phase which ultimately leads to phase separation.

Phase separation is associated to a negative charge compressibility $\kappa = \partial n / \partial \mu$, which corresponds to a negative curvature of the energy as a function of density (or equivalently on doping). In order to detect phase separation we need to solve the system for various values of Ca concentration and analyze the curvature of the ground state energy around the experimentally relevant case $x = 0.25$. In our case each of the independent solutions (FM, AFM, non magnetic) has the correct positive curvature for every value of x (see curves in the two inset of Fig. 4). However, when two curves cross as a function of doping and the system undergoes a first-order transition from one phase to the other, the energy has a cusp, and, more importantly, one can lower the energy by dividing the system into a fraction of AFM and a fraction of FM. This is realized through a Maxwell construction (solid black line in the two panels) and physically corresponds precisely to phase separation.

In Fig.4 we show the pressure vs Ca doping phase diagram obtained with DMFT.

At zero pressure we find phase separation between AFM and FM only close to $x = 0$ [34]. Our simplified model shows indeed phase separation below $x \simeq 0.16$, while larger doping correspond to homogeneous FM phases. Increasing the pressure increases the phase sep-

arated region, pushing its boundary to larger doping. At $P \simeq 5$ GPa the phase separation region reaches $x = 0.25$. Further increasing pressure at fixed x enhances the size of the AFM fraction of the system. Despite the simplifications introduced in our model, the characteristic pressure leading to phase separation is reproduced accurately by the theoretical calculations, confirming that the enhancement of the AFM superexchange can indeed account for the observed pressure-driven phase separation.

In summary, the pressure dependence of the magnetic temperature $T_C(P)$ was obtained up to 8 GPa and found to be rather close to $T_{IM}(P)$, suggesting that DE model still holds at HP. The reinforced role of SE localizing mechanism, competing with delocalizing DE, was confirmed by $T_C(P)$ and by the onset of an AFM state at low temperature. The novel antiferromagnetic structure is not related to the crystalline structure associated to the FM phase and observed at ambient pressure. The data are consistent with a picture in which lattice compression simultaneously induces both AFM order and a separation between two isostructural nuclear phases. The simultaneous appearance of FM and AFM peaks depicts a phase separation scenario promoted by pressure. This tendency towards a phase separation is properly reproduced, using a simplified theoretical model indicating that formation of domains is promoted by pressure.

Acknowledgments

M.C. is funded by the European Research Council under FP7/ERC Starting Independent Research Grant "SUPERBAD" (Grant Agreement n. 240524) and MIUR PRIN 2007 Prot. 2007FW3MJX003.

[1] E. Dagotto *et al.* Physics Reports **344**,1-153 (2001)
[2] S.-W. Cheong and H. Y. Hwang, in Colossal Magnetoresistance Oxides, edited by Y. Tokura, Monographs in Condensed Matter Science (Gordon and Breach, Reading, U.K., 2000).
[3] S. Jin *et al.*, Science **264**, 413 (1994)
[4] C. Zener, Phys. Rev. **82**, 403 (1951)
[5] A. J. Millis, Nature **392**, 147 (1998)(London); A. J. Millis *et al.*, Phys. Rev. Lett. **74**, 5144 (1995).
[6] I. Loa *et al.*, Phys. Rev. Lett. **87**,125501 (2001)
[7] A. Congeduti *et al.*, Phis. Rev. Lett.**86**, 1251 (2001)
[8] P. Postorino *et al.*, Phys. Rev. Lett. **91**, 175501 (2003)
[9] H. Y. Hwang *et al.*, Phys. Rev. B **52**, 15046 (1995)
[10] V. Laukhin *et al.*, Phys. Rev. B **56** R10009(1997)
[11] C. Cui *et al.*, Phys. Rev. B **68** 214417 (2003)
[12] C. Cui *et al.*, Phys. Rev. B **70** 094409 (2004)
[13] A. Congeduti *et al.*, Phys. Rev. B **63**, 184410 (2001).
[14] D. Feinberg *et al.*, Phys. Rev. B **57** R5583 (1998); M. Capone *et al.*, Europhys. J. B **17**,103 (2000)
[15] A Sacchetti, *et al.*, New J. Phys. **8**, 3 (2006)
[16] D. P Kozlenko *et al.*, J. Magn. Magn. Mater. **258**, 290 (2003)
[17] D. P. Kozlenko *et al.* JETP Letters **82**, 447 (2005)
[18] Y. Ding *et al.*, Phys. Rev. Lett. 102, 237201 (2009)
[19] E. Dagotto, New J. Phys. **7**, 67 (2005)
[20] A. Sacchetti *et al.*, Phys. Rev. Lett. **96**, 035503 (2006)
[21] L. Malavasi *et al.*, App. Phys. Lett. **94**, 061907 (2009)
[22] M. Baldini *et al.*, Phys. Rev. B **80**, 045123 (2009)
[23] I. N. Goncharenko, High Press. Res. 24, **193** (2004)
[24] P. G. Radaelli *et al.*, Phys Rev. B **56**, 8265 (1997)
[25] S. Landsgesell *et al.*, Phys. Rev. B **80**, 014412 (2009)
[26] http://www.ill.eu/sites/fullprof/
[27] L. Pinsard-Gaudart *et al.*, Phys. Rev. B **64**, 064426 (2001)
[28] P. M. Woodward *et al.*, Chem. Mater. **10**, 3652 (1998)
[29] L. Malavasi *et al.*, J. Mater. Chem. **10**,1304 (2010)
[30] A. B. Beznosov *et al.*, Phys. Rev. B **68**, 054109 (2003).
[31] M. Capone and S. Ciuchi, Phys. Rev. B, **65**, 104409 (2002).
[32] A. Georges *et al.*, Rev. Mod. Phys. **68**, 13 (1996)
[33] M. Capone, L. de' Medici, A. Georges, Phys. Rev. B **76**, 245116 (2007).
[34] R. S. Fishman *et al.*, New J. Phys. **8**, 116 (2006).
[35] Details of the calculations and a comparison with more realistic models of the manganites (inclusion for orbital degeneracy of the e_g electrons and proper JT interaction, quantum description of t_{2g} spins) will be presented in a forthcoming work.